RESEARCH ARTICLE | FEBRUARY 20 2025

Experimental investigation of the impact of directional distribution on the geometric characteristics of focused waves in finite water depth

Yanli He (赫岩莉); Zhe Gao (高哲) ; Lei Wang (王磊) ; Jinxuan Li (李金宣) ; Guohai Dong (董国海)

Physics of Fluids 37, 027175 (2025)
https://doi.org/10.1063/5.0249786

Physics of Fluids ARTICLE pubs.aip.org/aip/pof

Experimental investigation of the impact of directional distribution on the geometric characteristics of focused waves in finite water depth

Cite as: Phys. Fluids **37**, 027175 (2025); doi: 10.1063/5.0249786
Submitted: 20 November 2024 · Accepted: 6 January 2025 ·
Published Online: 20 February 2025

Yanli He (赫岩莉),[1,2] Zhe Gao (高哲),[3] Lei Wang (王磊),[2,4,a)] Jinxuan Li (李金宣),[2] and Guohai Dong (董国海)[2]

AFFILIATIONS

[1]College of Ocean Engineering and Energy, Guangdong Ocean University, Zhanjiang, 524088, China
[2]State Key Laboratory of Coastal and Offshore Engineering, Dalian University of Technology, Dalian 116024, China
[3]School of Marine Science and Engineering, Guangzhou International Campus, South China University of Technology, Guangzhou, 511442, China
[4]Department of Civil and Environmental Engineering, The Hong Kong Polytechnic University, Hong Kong, China

[a)]Author to whom correspondence should be addressed: wangleimme@scut.edu.cn

ABSTRACT

In actual wave fields, short-crested behavior is typically observed due to the superposition of wave components with varying wave frequencies and directional distributions. However, most of previous studies have simplified these as two-dimensional waves, neglecting the impact of directional distribution and leading to an incomplete understanding of its influence on nonlinear characteristics. This study investigates multi-directional focused waves with a single frequency in a laboratory setting. The comparison reveals that, unlike wave frequency, the vertical asymmetry factor influenced by directional distribution is linked to the variation in the period from zero-upcrossing to the crest. In multi-directional waves, the wave steepness defined for unidirectional waves is inadequate for measuring nonlinearity. There can be instances where the ratio of the subsequent envelope height at half the characteristic period to the preceding one exceeds 1, indicating a configuration highly prone to extreme events, especially with wider directional distributions. Furthermore, the deviation of the higher-order energy ratio from the theoretical solution increases with wave steepness (defined for the corresponding unidirectional waves) when the directional distribution is relatively concentrated, but no clear conclusion is reached at the directional distribution with $\theta_{max} = 60°$. This suggests that multi-directional waves, particularly with θ_{max} greater than 45°, warrant more attention as a critical inflection point. These findings provide a reference for future research on multi-directional, multi-frequency wave components.

I. INTRODUCTION

Surface gravity waves are the most prevalent type of waves in the ocean and serve as real-time manifestations of oceanic wave activity. These waves enhance ocean dynamics by inducing movement variations between the surface and particles, playing a crucial role in the transmission of ocean energy. In natural sea states, oceanic waves consist of components with varying frequencies and directional distributions.[1] However, in certain laboratory experiments, the wave field is often simplified to a two-dimensional model, and a simplification is also applied in small-scale field studies or during individual wave-breaking events. This approach overlooks the role of directional distribution,[2] which has been shown to significantly affect linear focusing effects and nonlinear wave–wave interactions[3,4] leading to notable changes in geometric characteristics. Focused waves are particularly valuable for investigating extreme wave characteristics in laboratory settings due to their easily controllable conditions. Therefore, examining the influence of directional distribution in focused waves is essential for a deeper understanding of wave propagation and evolution in the ocean, and for accurately predicting wave loads on marine engineering structures.

An extreme wave, often termed a catastrophic wave in the ocean,[5,6] is characterized by an unexpectedly large individual wave[7] and has attracted significant attention from scholars.[8] This type of wave is distinguished by concentrated energy,[9,10] strong nonlinearity,[11,12] and sudden

appearance,[13,14] posing a substantial threat to the safety of marine structures and ocean engineering.[15,16] The generation mechanisms are attributed to various factors, including modulation instability,[17,18] dispersive focusing,[14,19] abrupt topography,[20,21] wave–current interactions,[22,23] and crossing bimodal systems.[24,25] Among these, focusing is considered a primary method for addressing external influences such as wind, current, and topography, and is frequently employed in experimental laboratories.[26–30] Consequently, three-dimensional focused waves are central to ocean engineering and fluid dynamics research.

Significant progress has been made in understanding the nonlinear characteristics of oceanic waves. Under the ideal linear assumption, wave height is twice the amplitude, with symmetrical crests and troughs.[31] However, in reality, nonlinear interactions between waves during propagation result in energy transfer,[32,33] leading to nonlinear behavior[34–36] that manifests as asymmetry in the vertical and horizontal profiles, deviating from linear predictions. This includes a steeper crest and flatter trough.[26] To quantify these asymmetries, Myrhaug and Kjeldsen[37] introduced the vertical asymmetry factor to measure the ratio between the period from zero-upcrossing to the crest and the period from the crest to zero-downcrossing, reflecting the compression of waves in the temporal domain; the horizontal asymmetry parameter was proposed to describe the ratio of the envelope height at half the characteristic period to the envelope maximum,[4,35] reflecting the pressure difference caused by the sheltering effect on the preceding and following sides of the wave crests.[31] Additionally, the trough-to-crest ratio[38] was used to assess asymmetry between wave crests and troughs, resulting from the higher-order effects.[31] For a larger wave (characterized by greater wave amplitude), the vertical asymmetry parameter typically exceeded 1, indicating that the period of the following crest is longer than that of the preceding crest.[39] As wave amplitude increased, the vertical asymmetry parameter tended to increase,[31] enhancing the asymmetry between wave crests and troughs. This effect was attributed to the second-order bound waves,[40] which slightly steepened the preceding side of the wave crest and flattened the following side.[41] When a wave approached the critical state or reached breaking, the trough-to-crest ratio was asymptoted to 2.0, demonstrating that the crest was nearly twice the trough's height, with the crest tilting forward.[38,42] The crest steepness, defined as the ratio of the crest value to the length it spans, exhibited oscillatory growth before reaching a maximum value. This geometry of the crest is closely related to strong nonlinear characteristics.[43] In some cases, the preceding envelope height at half of the characteristic period was significantly less than the following envelope height.[4,35] Additionally, frequency is another crucial factor in oceanic waves.[30] Configurations with narrower spectral bandwidth were more likely to produce larger waves,[44] due to enhanced nonlinearity,[26] such as the triggering of higher-order harmonics and the activation of resonance effects.[32] In wave focusing, linear dispersion concentrated energy among various wave components, transforming the wave profile from a forward-leaning state to a symmetric form.[45] While, resonant nonlinearity, caused by the redistribution of the underlying spectrum, could result in wave profiles that were significantly higher and steeper than those predicted by linear and second-order theoretical models.[32]

Most of the studies above primarily focus on two-dimensional wave states and often overlook the impact of directional distribution, one of the controlling variables concerning the real sea state, which has been shown to influence nonlinearity significantly,[46] and alter local dynamics.[47] Generally, researchers have found that a wider directional distribution of waves tends to result in reduced nonlinearity,[48–50] thereby decreasing the probability of large wave events.[51,52] Recently, it has been observed that an increase in directional distribution can weaken spectral evolution and limit energy transfer.[53] However, some research has suggested that specific directional distributions can produce varying outcomes. Onorato *et al.*[54] discovered that the crossing angles between 10° and 30° are particularly susceptible to freak waves in crossing sea areas. Some nonlinear statistical parameters have been noted to increase in sea states with crossing angles between 40° and 60°.[47,55] Petrova and Guedes Soares,[56] demonstrated that spectral broadening in the high-frequency range for crossing sea areas with a 90° angle deviates from the trends observed at other angles. Sabatino and Serio[57] showed that crossing sea states can induce extreme waves, which are a significant cause of maritime accidents in severe weather. Furthermore, experimental findings by McAllister *et al.*[58] indicated that crossing sea areas with angles between 60° and 120° can generate waves as steep as or steeper than the Draupner wave (whose wave was 25.6 m high, with an 18.5 m crest in a significant wave height sea of almost 12 m recorded at Draupner platform in North Sea on 1 January 1995[59]).

Although numerous studies have examined the influence of wave amplitude and frequency on geometric characteristics of wave profiles, the impact of the most critical variable of three-dimensional waves—the directional distribution—remains the least understood. To address this gap, the dedicated multi-directional focused waves are simulated in the laboratory in this study. Our work brings two novel contributions. First, several asymmetric parameters of the wave profile influenced by the directional distribution independently are compared to that by wave frequency, covering the vertical asymmetry factor, the horizontal asymmetry parameter, and the trough-to-crest ratio. Second, the ratio of higher-order harmonic energy is analyzed to explain the variation of the asymmetric parameters.

The structure of this paper is as follows: Sec. II introduces the experimental setup and the analyzed parameters. Section III describes three asymmetric parameters of the wave profile influenced by directional distributions and wave frequencies. Section IV analyzes the spectral energy in different configurations. Finally, the conclusions are summarized in Sec. V.

II. EXPERIMENTAL SETUP AND ANALYTICAL PARAMETERS

A. Experimental arrangement

In this study, uni-frequency and multi-directional waves were experimentally focused in the multifunctional wave basin at the State Key Laboratory of Coastal and Offshore Engineering, Dalian University of Technology, as depicted in Fig. 1. The wave basin measures 55.0 m in length and 34.0 m in width. It has a working water depth of 0.5 m. A wavemaker, composed of a series of wave plates, is positioned on the left side of the basin to generate the specified multi-directional waves. An absorption zone is located at the end of the basin and along the upper and lower sides to reduce the wave reflections. The absorption coefficient reaches up to 90% for waves generated by the wavemaker. Consequently, a series of similar multi-directional waves have been successfully simulated in this tank with minimal or no influence from reflection.[60,61] As illustrated in Fig. 1, five gauges were installed to record the wave surface elevation, with gauge

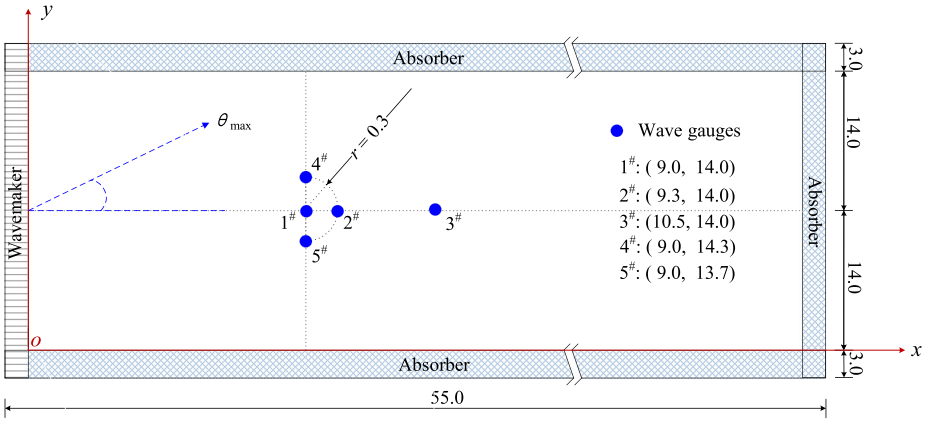

FIG. 1. Top view of the wave basin and pre-set experimental arrangement (unit: m).

1 positioned at the focused point $(x_b, y_b) = (9.0\ \text{m}, 14.0\ \text{m})$. Each gauge has an accuracy of ± 1 mm. For the forthcoming experiments, a sampling frequency of 100 Hz was employed.

It is well known that due to nonlinear interactions during wave propagation, the actual focused position can deviate from the assumed one,[26,62] with the extent of this deviation being unknown. To compare different nonlinear characteristics across various wave groups at the same location, we adjusted the wavemaker input parameters to focus waves from multiple directions at the same position irrespective of the wave configuration in this study. The defined or assumed focused position coincides with the actual focused position, specifically at gauge 1 $(x_b, y_b) = (9.0\ \text{m}, 14.0\ \text{m})$. Given that the end side of the wave basin is away from the focused position, we cease wave generation once the wave passes by the focused position and a sufficient number of samples have been collected. This approach shortens the time required for the water surface to flatten and reduces the interference from reflected waves. To ensure the accuracy and repeatability of the test results, 2–3 repeated wave generation processes are conducted once the corrected input parameters are established.

B. Wave configuration

The multi-directional waves with a uni-frequency are tested to be focused at a fixed position $(x_b, y_b) = (9.0\ \text{m}, 14.0\ \text{m})$. Detailed parameters are listed in Table I, where f denotes the wave frequency and A represents the focused amplitude. A total of 100 component waves are uniformly distributed from $\theta_{\min}$ to $\theta_{\max}$. To investigate the influence of directional distribution on nonlinear characteristics, Cases 1, 3, and 5 are compared. Additionally, Cases 2, 3, and 4 are analyzed to examine the impact of wave frequency. The detailed input parameters for different directional distributions are illustrated in Fig. 2.

C. Analytical parameters

1. Asymmetric parameters of the wave profile

Figure 3 presents the wave surface elevation over the time series. To quantify different aspects of the nonlinearity of the wave profile, three asymmetric parameters are employed: the vertical asymmetry factor λ, the horizontal asymmetry parameter β, and the trough-to-crest ratio.

a. Vertical asymmetry factor λ. The vertical asymmetry factor λ, proposed by Myrhaug and Kjeldsen,[37] has also been successfully utilized by Wu and Nepf[63] and Guedes Soares *et al.*[31] It is defined as

$$\lambda = \frac{t_{cf}}{t_{cp}}, \tag{1}$$

where t_{cp} represents the period from the zero-upcrossing to the crest, and t_{cf} denotes the period from the crest to the zero-downcrossing. Ideally, the wave profiles of the regular waves are vertically symmetric, meaning that t_{cp} equals t_{cf}, resulting in λ being equal to 1. As nonlinearity increases, the shapes of the crests and troughs change, leading to a divergence between t_{cp} and t_{cf}, which causes λ to deviate from 1. When λ exceeds 1, the unfocused time is greater than the focused

TABLE I. Detailed configuration of the multi-directional waves with uni-frequency focusing ($h = 0.5$ m).

Case	$[\theta_{\min}, \theta_{\max}]$ (°)	f (Hz)	A (m)
Case 1_1			0.08
Case 1_2	[−30, 30]	1.0	0.12
Case 1_3			0.14
Case 2_1			0.08
Case 2_2	[−45, 45]	0.9	0.12
Case 2_3			0.14
Case 3_1			0.08
Case 3_2	[−45, 45]	1.0	0.12
Case 3_3			0.14
Case 4_1			0.08
Case 4_2	[−45, 45]	1.2	0.12
Case 4_3			0.14
Case 5_1			0.08
Case 5_2	[−60, 60]	1.0	0.12
Case 5_3			0.14

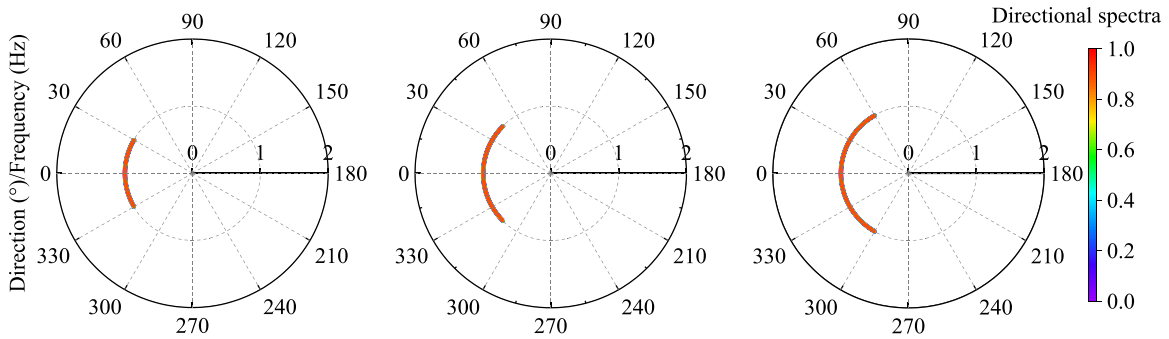

FIG. 2. Illustration of the normalized input spectra considering different directional distributions. (a) Case 1_1 ($\theta_{max} = 30°$), (b) Case 3_1 ($\theta_{max} = 45°$), and (c) Cases 5_1 ($\theta_{max} = 60°$).

time. Conversely, when λ is less than 1, the focused time is greater than the unfocused time.

b. Horizontal asymmetry parameter β. The horizontal asymmetry parameter β is defined as the ratio of the envelope height at half characteristic period (B_p or B_f) to the envelope maximum (η_c).[4,35,64] It is expressed as

$$\beta_p = \frac{|B_p|}{|\eta_c|}, \quad \beta_f = \frac{|B_f|}{|\eta_c|}, \tag{2}$$

where the subscripts p and f represent the preceding and the following, respectively.

The horizontal asymmetry, resulting from a sheltering effect that creates a pressure difference between the preceding and following sides of the crests,[41] has been shown to correlate strongly with front steepness.[31,40] The largest waves typically exhibit asymmetry with forward-leaning crests,[65] a characteristic feature of each crest in naturally occurring, unsteadily evolving dispersive nonlinear water wave groups.[66]

c. Trough-to-crest ratio. The trough-to-crest ratio, such as $|\eta_{tp}/\eta_c|$ and $|\eta_{tf}/\eta_c|$, measures the asymmetry between the trough and the crest. For linear waves, the ratio is valued at 1. As wave nonlinearity increases, higher-order harmonics causes the crest steepened and the trough flattened, resulting in a trough-to-crest ratio of less than 1.

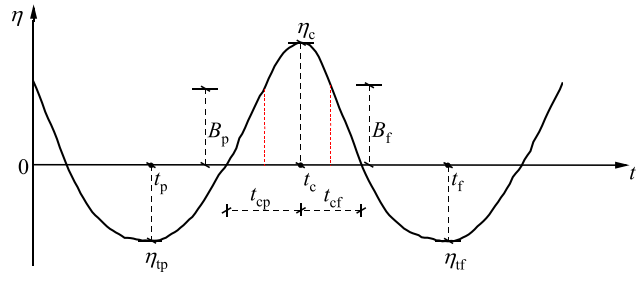

FIG. 3. Illustration of the wave profile for Case 1_3 listed in Table I (θ_{max}=30°, f = 1.0 Hz, and A = 0.14 m).

2. Theoretical solutions

Well known, the surface elevation of uni-frequency waves at the position (x, y) based on linear theory can be expressed as

$$\eta(x, y, t) = A' \cos\theta, \tag{3}$$

where A' is the wave amplitude, θ ($=kx - \omega t$) is the phase, ω is the angular frequency, and k is the wave number obtained from the dispersion relation.

For the second-order theoretical solution in a working depth h, the expression can be written as[67]

$$\eta(x, y, t) = A'\left[\cos\theta + \frac{A'k}{4}\frac{\cosh kh(\cosh 2kh + 2)}{\sinh^3 kh}\cos 2\theta\right]. \tag{4}$$

The normalized theoretical solutions of regular waves as shown in Fig. 4 include the wave surface elevations and the corresponding energy spectra. T represents the wave period, and *norf* is the frequency normalized by the basic wave frequency. When considering the second-order terms, the total energy E can be separated into two components: the energy of linear part E_1 and the energy of second-order part E_2. Therefore, the variation of the ratio E_2/E (where $E = E_1 + E_2$) can be used to measure the changes in nonlinearity caused by different directional distributions or wave frequencies.

III. ASYMMETRICAL FEATURES AT THE FOCUSED POSITION

A. Wave profile

Wave surface elevation is a fundamental metric for investigating the characteristics of wave profiles. Figure 5 compares the wave surface elevation across various directional distributions and wave frequencies. In this figure, the horizontal axis represents the number of wave periods from the focused time, while the vertical axis denotes the wave surface elevation normalized by the maximum wave-crest height at the defined focused location (also the actual focused location in this study).

On the left panel, the differences caused by varying directional distributions and their variations with wave amplitude are illustrated. For smaller wave amplitude [Fig. 5(a-1)], as the wave directional distribution broadens from [−30°, 30°] (solid line) to [−60°, 60°] (dotted line), indicating a decrease in spreading concentration, the trough trends to become more symmetrical with the crest. Concurrently, the

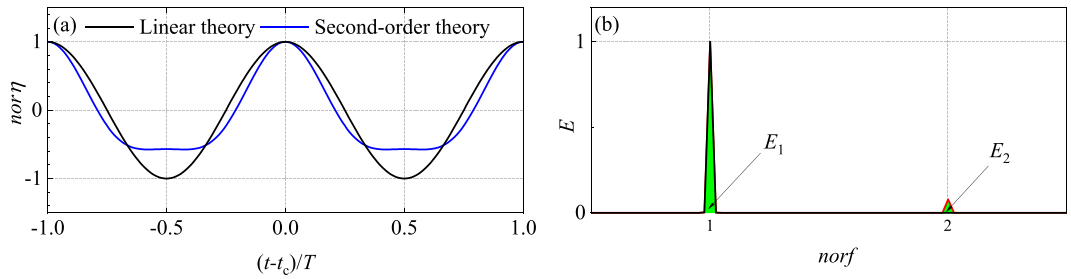

FIG. 4. The normalized theoretical solutions for the regular wave in the condition with $f = 1.0$ Hz and $A = 0.12$ m (that is, unidirectional wave corresponding to Cases 1_2, 3_2, and 5_2). (a) Wave surface elevations and (b) energy spectra.

asymmetry of the envelope height on the preceding and following sides of the wave crest changes, affecting the durations between zero-upcrossing or zero-downcrossing and the crest. As the focused amplitude increases [Fig. 5(a-2)], the troughs become flatter with minimal differences in their peaks, even though their appearances are delayed with widening directional distributions. The peak of the crest moves forward slightly, which will trigger some asymmetry of the wave profile. For even steeper waves [Fig. 5(a-3)], the trough-to-crest ratios can reach up to 0.6, accompanied by a prominent effect of directional distribution. This manifests as a greater delay in the appearance time of the trough peak and increased asymmetry in durations between zero-upcrossing or zero-downcrossing to the crest.

Regarding the effect of wave frequency [Fig. 5(b)], the directional distribution is fixed at [−45°, 45°]. For smaller focused amplitude [Fig. 5(b-1)], as the wave frequency increases from 0.9 to 1.2 Hz (i.e., the wavelength becomes shorter), the trough gradually becomes flatter and its value decreases. As the focused amplitude increases [Fig. 5(b-2)], the wave profile exhibits a steeper crest and flatter trough compared to the smaller focused amplitude. A slight difference in the peak of the trough can be observed with varying wave frequencies.

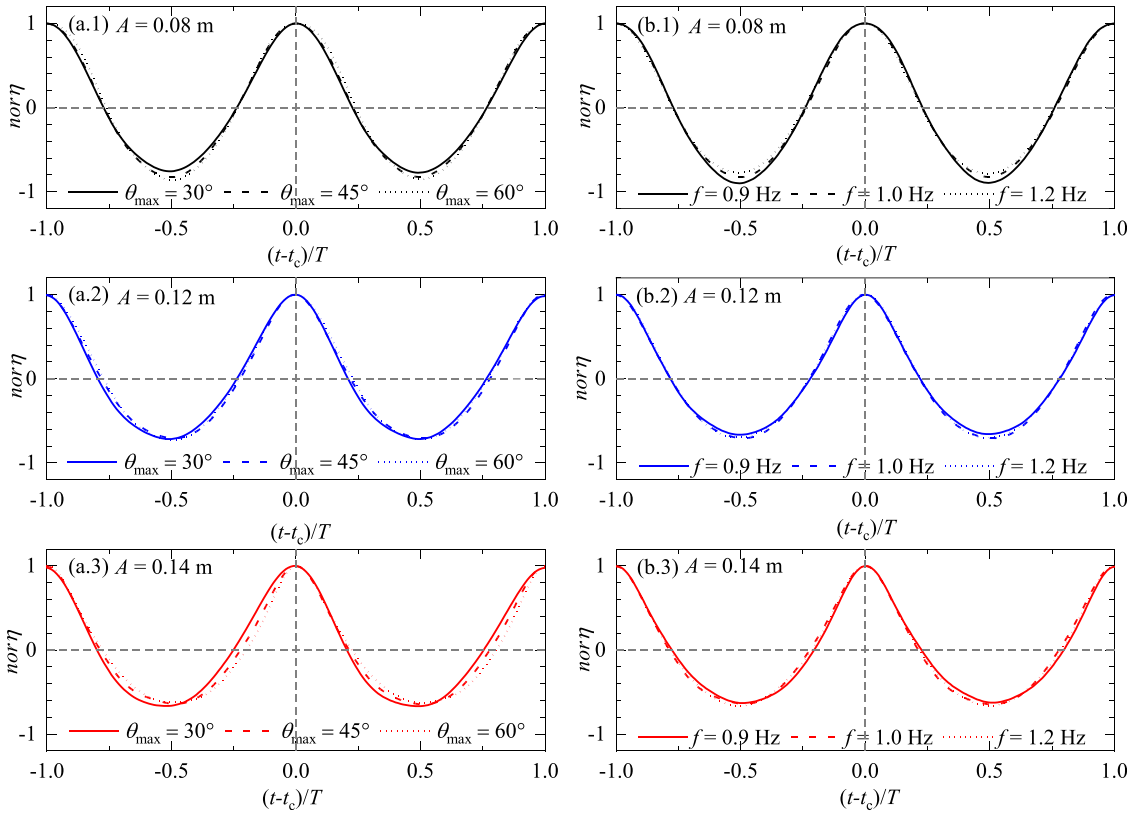

FIG. 5. Comparison of the normalized wave surface elevations at defined focused location (also actual focused location in this study), i.e., at gauge 1 (x_b, y_b) = (9.0 m, 14.0 m). (a) With various directional distributions (with fixed frequency $f = 1.0$ Hz) and (b) with various frequencies (with fixed directional distribution $\theta_{max} = 45°$).

For larger focused amplitude [Fig. 5(b-3)], the appearance time of the trough peak is minimally influenced by changes in wave frequency, which contrasts with the effect of directional distributions. Moreover, as the wavelength becomes shorter, the wave profile gradually exhibits forward leaning, which is considered a precursor to extreme wave events.

In summary, both directional distribution and wave frequency significantly impact the wave profile. These effects manifest as differences in asymmetrical durations between zero-upcrossing or zero-downcrossing to the crest (i.e., vertical asymmetry), wave forward leaning or backward leaning (i.e., horizontal asymmetry), and trough-to-crest ratio, which will be analyzed in Secs. III B–III D.

B. Vertical asymmetry factor

Figure 6 compares the variation of the preceding period from the zero-upcrossing to the crest t_{cp} and the following from the crest to the zero-downcrossing t_{cf}. On the left panel, for smaller focused amplitude [Fig. 6(a-1)], t_{cp} remains relatively consistent across different directional distributions, while the following period t_{cf} varies, with a larger value observed at $\theta_{max} = 60°$. This results in t_{cp} being slightly larger than t_{cf} for the other two directional distributions, indicating that a more concentrated directional distribution increases the likelihood of t_{cp} exceeding t_{cf}. For moderate focused amplitude [Fig. 6(a-2)], as the directional distribution broadens, t_{cp} decreases and then stabilizes, while t_{cf} exhibits an opposite trend, with t_{cp} consistently remaining above t_{cf}. For larger focused amplitude [Fig. 6(a-3)], t_{cp} decreases significantly with increasing directional distribution, with t_{cp} falling below t_{cf} at $\theta_{max} \in [-60°, 60°]$. Generally, the larger the focused amplitude, the greater the decrease in t_{cp} with increasing directional distribution, whereas the variation in t_{cf} remains stable, despite a slight decline in the corresponding values. This phenomenon is attributed to the reason that as the directional distribution increases, the wave energy concentration weakens, resulting in the crest speed decreasing due to the nonlinearity-dependent changes in dispersion.[45,62] Consequently, it leads to a significant reduction in the preceding period from the zero-upcrossing to the crest. Different phenomena are observed on the right panel. There is no uniform variation pattern of t_{cf} across various focused amplitudes with increasing wave frequency, with values mostly fluctuating around 0.23. Fascinating variations occur in t_{cp}. For smaller focused amplitude [Fig. 6(b-1)], t_{cp} first decreases slightly and then increases, consistently remaining above t_{cf}. As focused amplitudes increase [Fig. 6(b-2)], the trend gradually reverses, with t_{cp} initially increasing and then decreasing as the wave frequency increases. For larger focused amplitude [Fig. 6(b-3)], t_{cp} in a longer-wave condition (i.e., $f = 0.9$ Hz) is less than the corresponding t_{cf}, while in a shorter-wave condition (i.e., $f = 1.2$ Hz), these two periods are equivalent.

Figure 7 presents the variations in vertical asymmetry λ (the ratio of t_{cf} to t_{cp}) influenced by directional distributions and wave frequencies. The purple dashed line represents the symmetry predicted by

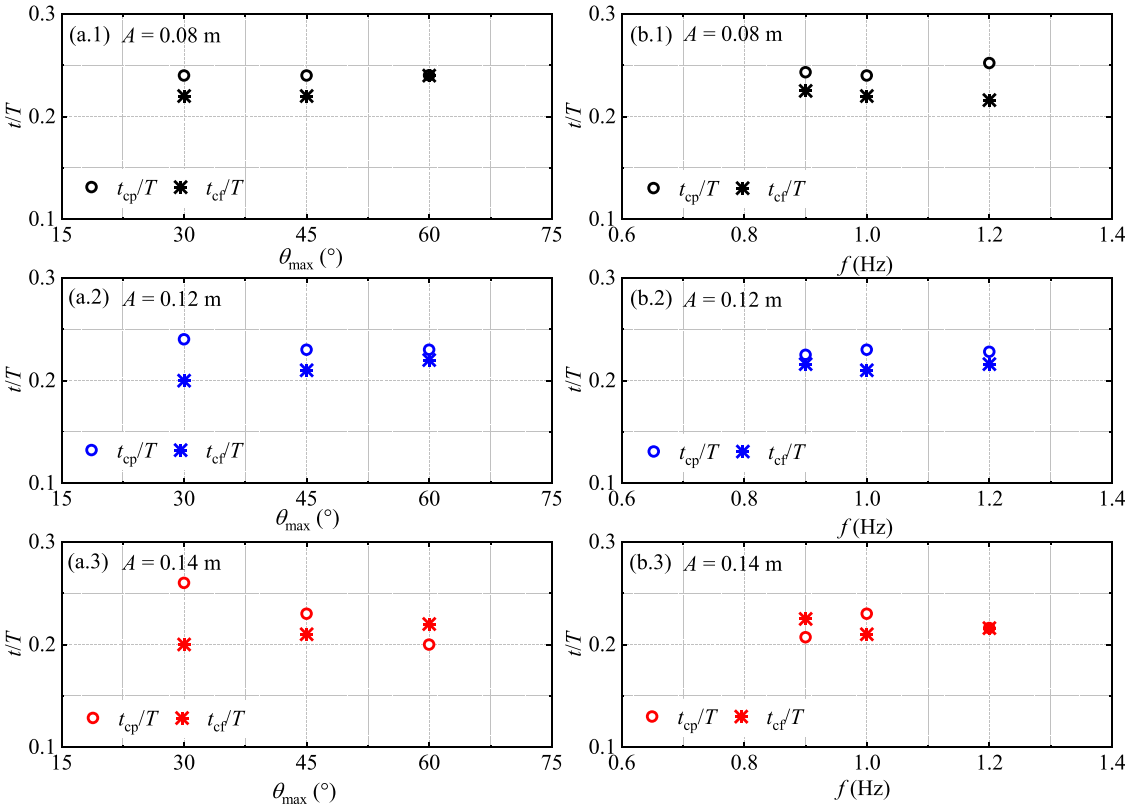

FIG. 6. Variation of the periods from zero-upcrossing to the crest and that from the zero-downcrossing to the crest. (a) With various directional distributions (with fixed frequency $f = 1.0$ Hz) and (b) with various frequencies (with fixed directional distribution $\theta_{max} = 45°$).

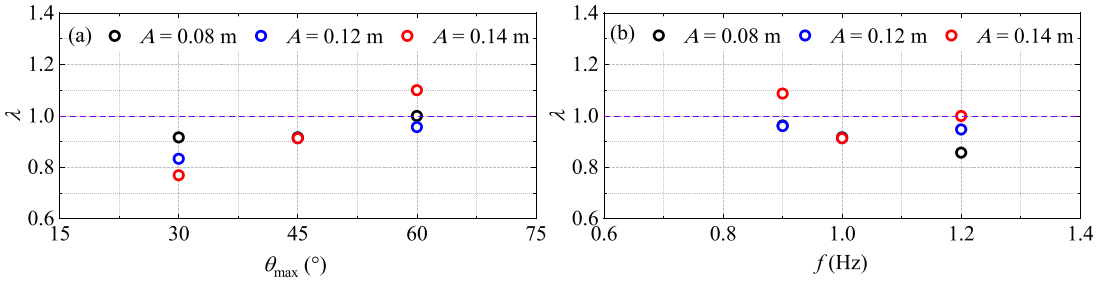

FIG. 7. Variation of the vertical asymmetry. (a) With various directional distributions (with fixed frequency $f = 1.0$ Hz) and (b) with various frequencies (with fixed directional distribution $\theta_{max} = 45°$).

linear theory for reference. In Fig. 7(a), for a smaller focused amplitude (represented by the black), λ gradually increases from less than 1.0 to approximately 1.0 as the directional distribution broadens. With increasing focused wave amplitude, λ continues to exhibit an increasing trend, but the magnitude of this increase varies. Specifically, λ exceeds 1.0 for $A = 0.14$ m, while it remains below 1.0 for $A = 0.12$ m. This indicates that the influence of focused amplitude on the variation of λ is related to the directional distribution. For the narrower directional distribution (i.e., more concentrated energy), λ gradually decreases with increasing focused amplitude but remains less than 1.0. This is attributed to an increase in t_{cp} despite a slight increase in t_{cf}. As the directional distribution widens, λ stabilizes at 0.91 across various focused amplitudes due to the stable corresponding t_{cf} and t_{cp} (Fig. 6). Beyond this point, no clear variation pattern is observed.

In Fig. 7(b), for a smaller focused amplitude, λ gradually decreases as the wave frequency increases. While for a larger focused amplitude, as the frequency increases, λ initially decreases and then increases. For longer waves (i.e., $f = 0.9$ Hz), λ remains nearly almost unchanged below 1 in configurations with small focused amplitudes ($A = 0.08$ m and $A = 0.12$ m). This is because, although both t_{cf} and t_{cp} decrease [Figs. 6(b-1) and 6(b-2)], the magnitude of their decrease is consistent. For shorter waves (i.e., $f = 1.2$ Hz), λ gradually increases to around 1 as the focused amplitude increases, indicating that the crest profile transforms from asymmetric to symmetric. The decline in t_{cp} meaning the shortened preceding period, driven by enhanced nonlinear effects, dominates the behavior, while t_{cf} remains constant [Fig. 6(b)]. This contrasts with the variations seen in unidirectional waves, where steeper waves display stronger nonlinearity and more pronounced nonlinear characteristics. In wave configurations with a fixed directional distribution at $\theta_{max} = 45°$, unique phenomena are observed.

As pointed out by She *et al.*,[68] the vertical asymmetry decreases with the increase in the directional distribution, and the variation is reversed when the directional distribution reaches up to $\theta_{max} = 60°$. This is consistent with the findings in multi-directional multi-frequency waves that the nonlinear effect can be weakened by the given directional distribution.[49] A more interesting conclusion is that the directional distribution and wave frequency are suggested to influence the variation of vertical asymmetry factor λ through different mechanisms. Under the influence of directional distribution, the variation in λ is primarily determined by changes in t_{cp}. While considering wave frequency, the variation in λ shows little dependence on the t_{cp} in the configuration with longer waves at $\theta_{max} = 45°$. Compared to these observation in the temporal domain, Perlin *et al.*[69] summarized similar conclusions in the spatial domain. As wave steepness increases, wave exhibits fore-aft asymmetry because of wave-crest front-face steepening.[69] The crest's geometric parameters are pointed to be more suitable for describing the local crest geometry and are of great significance for predicting extreme waves.[69] Although further research suggested that larger waves have larger coefficients of front steepness compared to back steepness, and larger coefficients of down-crossing steepness compared to up-crossing steepness,[31,40] it appears that up-crossing parameter has some correlation with front steepness. Yao and Wu[70] demonstrated that the limiting steepness and geometric parameters of the crest in extreme waves, determined from spatial surface profiles and temporal surface-elevation measurements, differ significantly. Therefore, spatial characteristics are not fully equivalent. Additionally, the wave configuration with a fixed directional distribution at $\theta_{max} = 45°$ presents unexpected results. While wave steepness predominantly governs nonlinearity, this specific directional distribution also exerts a significant impact.

C. Horizontal asymmetry parameter

Figure 8 compares the variation of the preceding horizontal asymmetry parameter β_p and the following horizontal asymmetry parameter β_f. In Fig. 8(a-1), for a smaller focused amplitude, both β_p and β_f increase as the directional distribution broadens, with β_p always below β_f. For a larger focused amplitude [Fig. 8(a-2)], β_p continues to increase, albeit at a reduced growth rate, while β_f exhibits a different trend, initially decreasing and then increasing. This results in the convergence of β_p and β_f at $\theta_{max} = 60°$. When the focused amplitude reaches 0.14 m, both β_p and β_f decrease with the increasing directional distribution, indicating more energy concentrated around the crest on both the preceding and following sides. From the analysis of field measurement conducted by Tang *et al.*,[35] β_p is pointed out to be less than β_f in extreme events. Additionally, the half-period before the crest is shorter than that after the crest, indicating the presence of nonlinear contraction of the wave group.[35]

Concerning the effect of wave frequency, as shown in Fig. 8(b), for a smaller focused amplitude, the crest tends to have a steeper profile in the following compared to the preceding. As wave frequency increases, β_p maintains a growth trend, while β_f decreases slightly, with β_p approaching β_f at 1.2 Hz. For larger focused amplitudes, the variation in β_p and β_f are not uniform. Notably, in the configuration with the frequency $f = 1.2$ Hz, these two values are quite close to each other, and the larger the focused amplitude, the smaller the value,

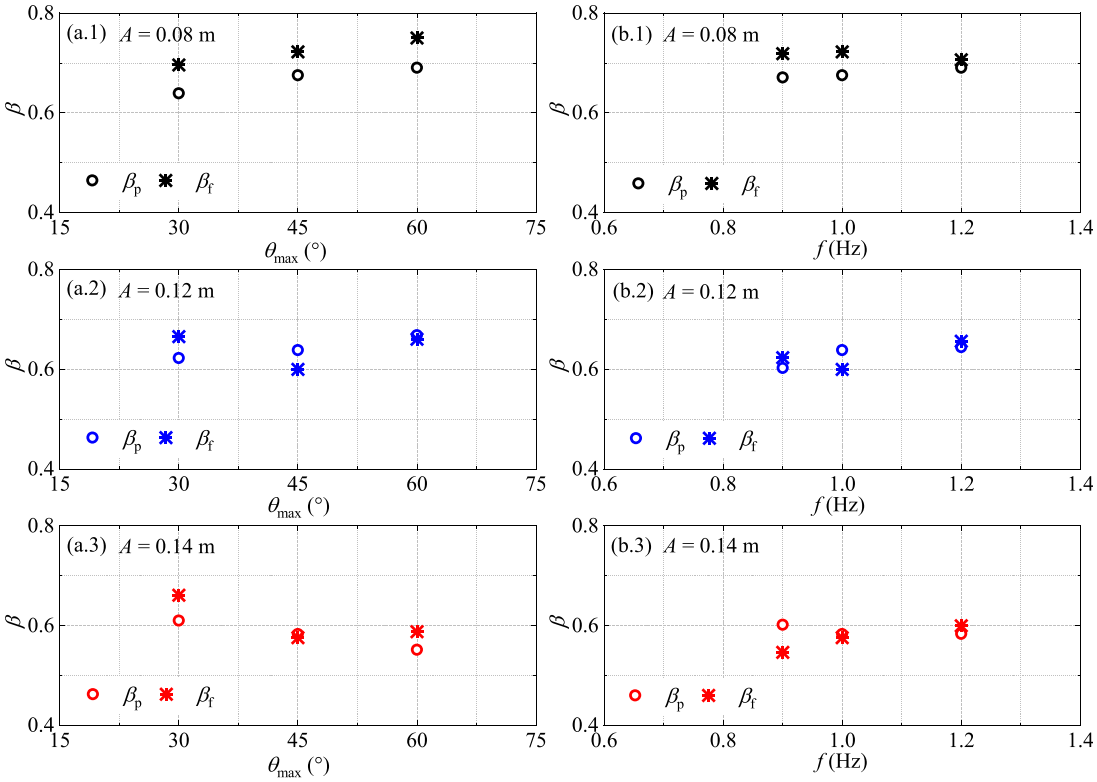

FIG. 8. Variation of the preceding and following horizontal asymmetry parameters. (a) With various directional distributions (with fixed frequency $f = 1.0$ Hz) and (b) with various frequencies (with fixed directional distribution $\theta_{max} = 45°$).

suggesting the wave crest increasingly compressed. Consequently, the compressed wave crest increases the crest steepness, resulting in more energy concentrated around wave crest on both preceding and following sides and the emergence of extreme wave characteristics.

Figure 9(a) explores the effect of the directional distributions on the ratio of the preceding to the following horizontal asymmetry parameters. For a smaller focused amplitude, this ratio remains relatively stable around 1.1, indicating a forward-leaning state, despite a decline in both β_p and β_f along the directional distribution [Fig. 8(a-1)]. This behavior is attributed to the higher energy concentration on the preceding side, resulting in greater pressure on the following side. As the focused amplitude increases, the ratio falls below 1.0 when θ_{max} is 45° and 60°, indicating a transition to a backward leaning wave crest due to more energy being concentrated on the following side. When the focused amplitude reaches 0.14 m, the ratio at $\theta_{max} = 60°$ returns to a value greater than 1.0. These observations challenge the conventional understanding that a wider directional distribution, which disperses energy more broadly, is less prone to extreme events. In specific configuration, the energy concentration on the following profile can exceed that of the preceding, thereby increasing the likelihood of extreme events.

Figure 9(b) illustrates the corresponding effect of the wave frequencies. The variation at $\theta_{max} = 45°$ does not follow the traditional trend where nonlinearity increases monotonically with wave steepness.

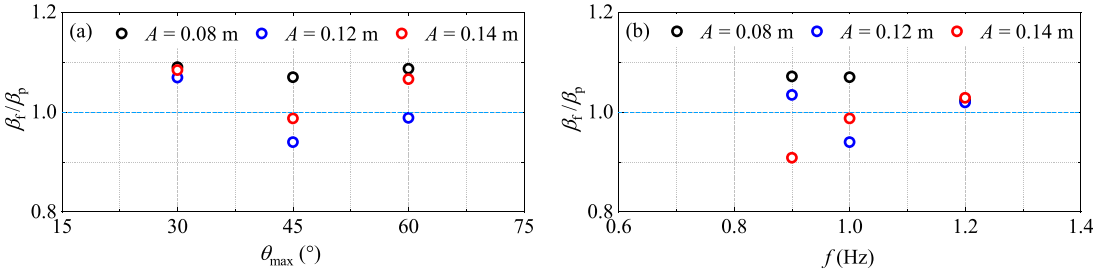

FIG. 9. Variation of the ratio of the preceding and following horizontal asymmetry parameters. (a) With various directional distributions (with fixed frequency $f = 1.0$ Hz) and (b) with various frequencies (with fixed directional distribution $\theta_{max} = 45°$).

Even for small focused amplitudes (e.g., $A = 0.08$ m), there is a potential for extreme events, as indicated by a ratio greater than 1.0 and a forward-leaning crest, regardless of wavelength. Surprisingly, for relatively longer waves (e.g., $f = 0.9$ Hz), steeper waves exhibit a smaller ratio, contrary to the behavior observed in unidirectional waves. This is primarily due to the rapid decrease in β_f, causing the crest transitions from forward leaning to backward leaning as nonlinearity increases with a fixed directional distribution of $\theta_{max} = 45°$.

Therefore, it is essential to consider the impact of multidirectional waves or even crossing waves on oceanic devices or equipment during oceanic activities, such as analyzing field measurements, predicting wave evolution, and assessing the load of the marine structure.

D. Trough-to-crest ratio

The trough-to-crest ratio is another parameter used to measure asymmetry, as illustrated in Fig. 10. In all four panels, the preceding and following troughs consistently coincident. This can be attributed to the fact that, despite being composed of wave components with varying directional distributions or frequencies, the wave maintains regularity with symmetrical troughs. However, the effects of directional distribution and wave frequency differ significantly. For smaller focused amplitude (indicated by the black markers), a narrower directional distribution (i.e., more concentrated energy) and a shorter wavelength (i.e., higher wave frequency) result in a smaller trough-to-crest ratio. This occurs because, in such configurations, higher-order harmonics due to enhanced nonlinearity can cause the crest to steepen and the trough to flatten.[31] This trend is consistent with observations in unidirectional waves. When the amplitude is moderate (i.e., $A = 0.12$ m), the trough-to-crest ratio decreases as the directional distribution increases, eventually approaching nearly equal values. For larger amplitude (i.e., $A = 0.14$ m), the trough-to-crest ratio decreases along the directional distribution, likely due to the effect of bound harmonics,[53] which result in steeper crests and flatter troughs. This finding also supports the assertion by McAllister *et al.*[58] that larger waves, such as Draupner wave, can also be generated in a crossing state with crossing angles between 60° and 120°.

However, as wave steepness increases, the anticipated enhancement (i.e., a decrease in the ratio) is not observed. Notably, for longer wave configurations [i.e., $f = 0.9$ Hz in Fig. 10(b)], the relation between increasing wave steepness and a decreasing ratio, which could indicate stronger nonlinearity, is stratified. As the frequency increases, unlike unidirectional waves, the trough-to-crest ratio does not show enhanced asymmetry between crests and troughs following nonlinear enhancement. This suggests that in real wave fields, which exhibit short-crested behavior and account for both wave frequencies and directional distributions, the effects of these factors are not a simple linear superposition. Therefore, in practical engineering applications, wave fields should not be simplified to unidirectional or even uni-frequency unidirectional waves when evaluating wave loads and other related effects.

IV. ANALYSIS OF HARMONIC ENERGY

Energy transfer is the essence of wave evolution. As nonlinear waves propagate, the nonlinear interactions between various wave components, such as wave–wave interactions, are excited.[62] This excitation results in higher-order harmonics that influence the spectral frequency[30] and lead to energy transfer.[71] Consequently, the dispersion relation is altered.[32] This process influences the deformations in the wave profile, including various asymmetries. To reveal the underlying physics, we will analyze harmonic energy ratios to explain on how the wave profile varies with different directional distributions and wave frequencies.

A. Energy spectra

Figure 11 compares the normalized energy spectra in various separated orders influenced by the directional distribution and wave frequency, including the linear components (the left column), second-order components (the middle column), and third-order components (the right column). A common phenomenon observed is the appearance of higher-order harmonics, including second- and even third-order

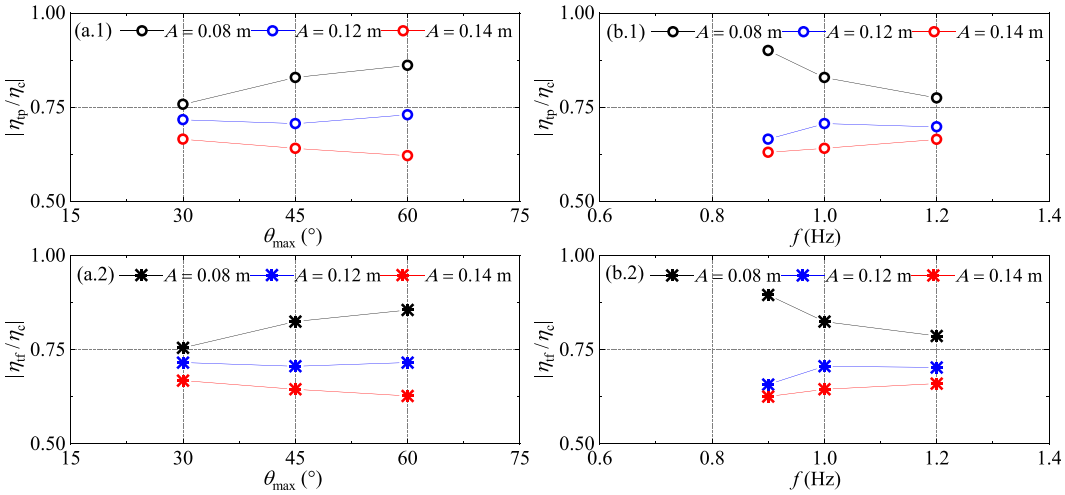

FIG. 10. Variation of the preceding and following trough-to-crest ratio. (a) With various directional distributions (with fixed frequency $f = 1.0$ Hz) and (b) with various frequencies (with fixed directional distribution $\theta_{max} = 45°$).

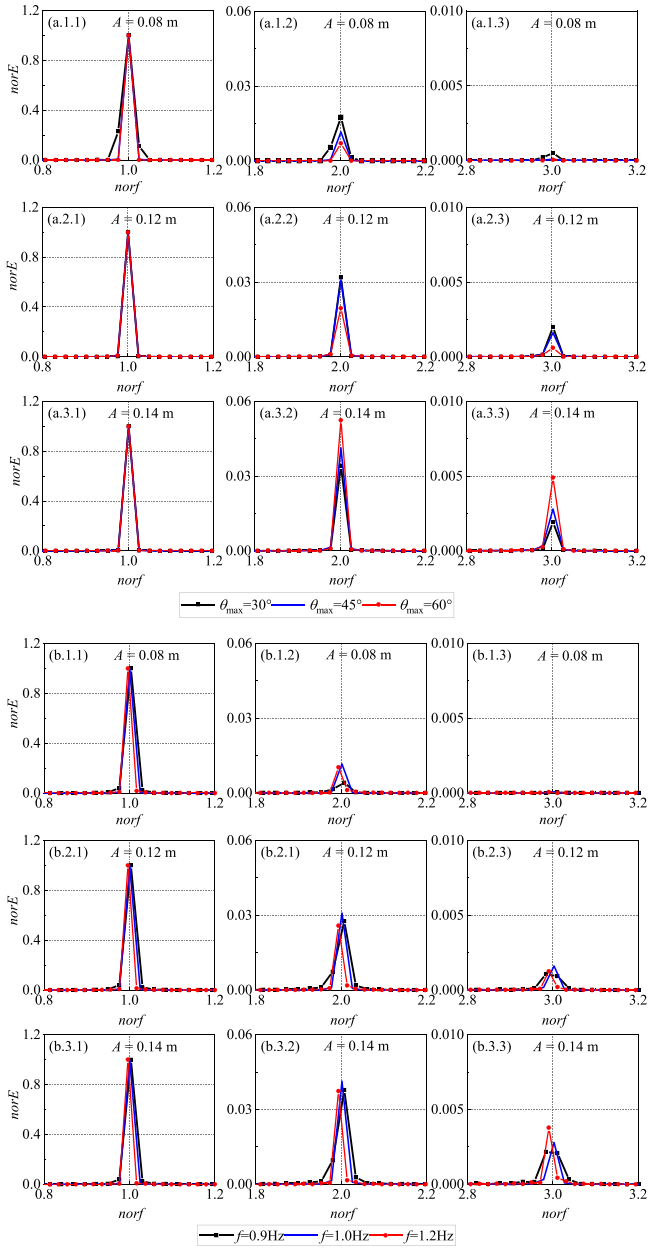

FIG. 11. Local magnification of normalized energy spectrum in various separated orders. (a) With various directional distributions (with fixed frequency $f = 1.0$ Hz) and (b) with various frequencies (with fixed directional distribution $\theta_{max} = 45°$).

harmonics. However, the effects of these two variables on the spectral peak and the corresponding frequency are quite different.

Regarding the impact of the directional distribution [Fig. 11(a)], for smaller focused amplitude [Fig. 11(a-1)], the proportion of the second- and third-order energy is greater for more concentrated directional distributions compared to moderately concentrated and least concentrated distributions. As the focused amplitude increases [Fig. 11(a-2)], the proportion of second- and third-order energy also increases. At $\theta_{max} = 30°$ and $\theta_{max} = 45°$, both ratios are nearly equal and higher than at $\theta_{max} = 60°$. This explains the variation of the trough-to-crest ratio [Fig. 10(a)], indicating that the relation between the trough-to-crest ratio and higher-order harmonics in unidirectional waves also applies to multi-directional waves in such condition. When the focused amplitude reaches 0.14 m [Fig. 11(a-3)], the second- and third-order energy ratios at $\theta_{max} = 60°$ surpass those at $\theta_{max} = 45°$ and at $\theta_{max} = 30°$. The increase in harmonic energy leads to nonlinear enhancement, resulting in a decrease in the trough–crest asymmetry, which is manifested as a smaller value of trough-to-crest ratio [Fig. 10(a)].

Under the influence of wave frequency [Fig. 11(b)], although the proportion of second- and third-order energy increases with the focused wave amplitude, wave frequency appears to have lesser effect on these proportions compared to the impact effect of directional distribution. For smaller focused amplitude [Fig. 11(b-1)], the energy ratio of the second-order harmonic is lower for relatively lower-frequency waves than for higher-frequency waves (e.g., $f = 1.0$ and 1.2 Hz). As the frequency increases, the proportion of second-order energy rises, consistent with the unidirectional waves. Additionally, the third-order energy remains close to zero across all frequencies. As the focused wave amplitude increases [Fig. 11(b-2)], both second- and third-order energy ratios show a noticeable increase. However, these ratios do not exhibit significant changes with increasing frequency, indicating that frequency has a minor impact on higher-order energy ratios for waves with moderate amplitudes. When the focused amplitude reaches $A = 0.14$ m [Fig. 11(b-3)], both second- and third-order energy ratios increase. While the second-order energy ratio remains relatively unchanged with frequency, the third-order energy shows a slight increase, although this increase is not substantial.

The results indicate that the mechanism by which directional distribution and frequency affect the ratio of higher-order energy differ. For large amplitudes, unlike unidirectional waves, an increase in directional distribution leads to a significant rise in bound wave energy resulting in a shallower trough. Conversely, as frequency increases, the harmonic energy ratio remains nearly constant, which contradicts the expected nonlinear relationship between two-dimensional waves and harmonic energy growth. This discrepancy may be because the results in Fig. 11(b) are based on an analysis at $\theta_{max} = 45°$. These differing variation patterns suggest that the impact mechanism driven by various directional distributions is complex and non-monotonic for both second- and third-order energy, contrasting with the relatively straightforward influence of wave frequencies.

B. Ratio of higher-order harmonic energy

The energy changes caused by the continuous directional distribution are not monotonic. To investigate this expansion of this phenomenon, we introduce the theoretical solution of unidirectional waves that we are familiar with as a comparison. The variation of the energy ratio of second-order terms is shown in Fig. 12. The crosses represent the theoretical values, and the hollows represent the experimental data. Different colors denote different configurations. First, compared to the results of unidirectional waves, the proportion of second-order energy in multi-directional waves has sharply reduced, irrespective of the directional distribution or wave frequency. This reflects that directional distribution does indeed weaken energy

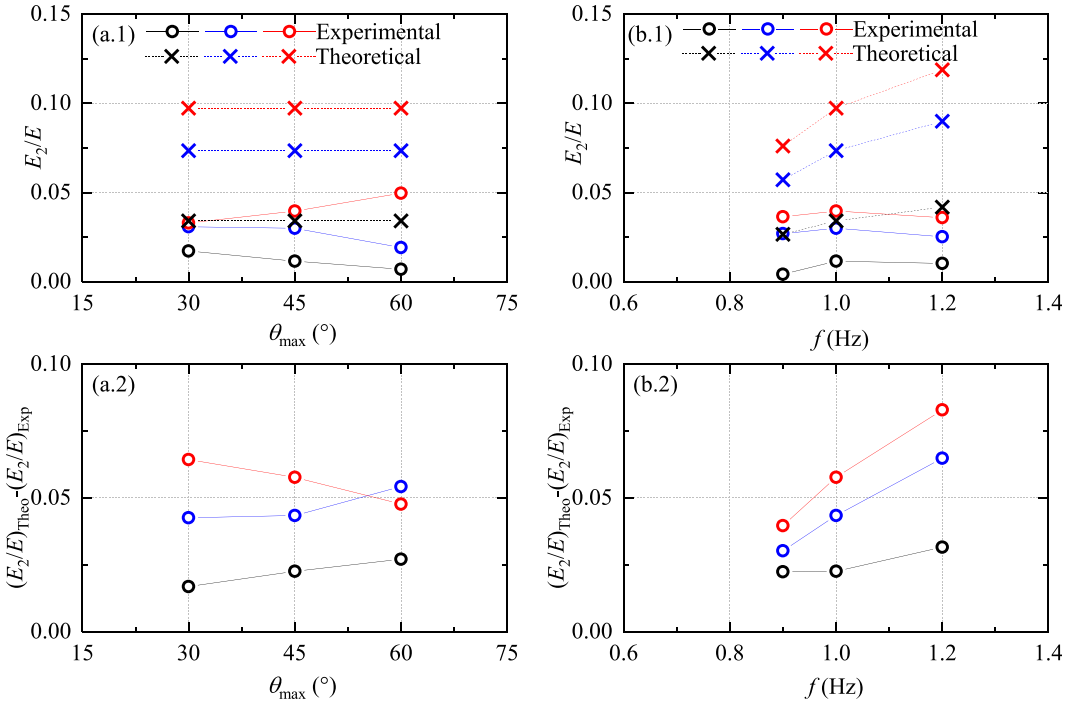

FIG. 12. Variation of the energy ratio of second-order terms. (a) With various directional distributions (with fixed frequency $f = 1.0$ Hz) and (b) with various frequencies (with fixed directional distribution $\theta_{max} = 45°$). The hollows and crosses denote the experimental and theoretical results, respectively. ($A = 0.08$ m: black color; $A = 0.12$ m: blue color; and $A = 0.14$ m: red color).

concentrations to a certain extent in our given configuration than unidirectional waves.

In Fig. 12(a-1), as the focused amplitude increases, the nonlinearity of unidirectional waves is enhanced, manifested as a rapid increase in the proportion of second-order energy in the theoretical solution. For smaller focused amplitude (represented by the black), as the directional distribution broadens, the deviation from the theoretical prediction becomes larger, indicating that the second-order energy rapidly reduces. When the focused amplitude equals 0.12 m (represented by the blue), the deviation increases quickly and becomes larger with the widening of the directional distribution. A different phenomenon happens when the focused amplitude reaches up to 0.14 m (represented by the red)—the more concentrated the directional distribution, the greater the energy ratio offset. As the directional distribution becomes wider, the energy ratio shift becomes smaller and smaller [also can be observed in Fig. 12(a-2)], which is inconsistent with our conventional hypothesis. If this phenomenon could be explained as wave breaking, at least the energy ratio at $\theta_{max} = 30°$ should be lower than that with a smaller focused amplitude, while here the ratio at $\theta_{max} = 60°$ is much smaller. Moreover, McAllister *et al.*[1] recently also pointed out that the steepness of the three-dimensional waves before breaking may be twice that of traditional two-dimensional waves. Hence, it should be attributed to the unusual role of the directional distribution. That is, the impact of the directional distribution is not monotonic, which is related to the focused amplitude (i.e., the steepness of the unidirectional waves). Concerning the influence of the wave frequency [Fig. 12(b)], although the second-order energy ratio first increases and then decreases with increasing frequency (i.e., shortened waves), compared to the theoretical difference [Fig. 12(b-2)], it monotonically increases with increasing frequency. The case with larger focused wave amplitudes always stays above that with smaller amplitudes. This variation does not conflict with that observed in Fig. 12(a), as it is fixed under the configuration of $\theta_{max} = 45°$.

Additionally, the variation of the third-order energy ratio is given in Fig. 13. Generally, the energy ratio of the third-order harmonics is one order of magnitude smaller than that of second-order harmonics. This can also be found from Fig. 11, where the vertical axes of the second- and third-order energy ratio differ significantly. Moreover, irrespective of the influence of directional distributions or wave frequencies, the trend of the energy ratio of third-order harmonic under different local wave amplitudes is quite similar. It should be noted that, in a multi-directional configuration, the third-order harmonic is influenced not only by amplitude and frequency but also by directional distribution, unlike the second-order harmonic. Additionally, the third-order harmonic can cause a frequency shift, which does not occur in the second-order solution. Even with a theoretical solution for the third-order harmonic, it is challenging to identify the dominant factors. Therefore, theoretical values are not provided for comparison in this study.

From Fig. 13, the variation of the higher-order energy ratio relative to the theoretical solution increases with the enhancement of the wave steepness corresponding to unidirectional waves when the directional distribution is relatively concentrated (i.e., $\theta_{max} = 30°$ and $\theta_{max} = 45°$ in this given configuration). Still, there is no clear

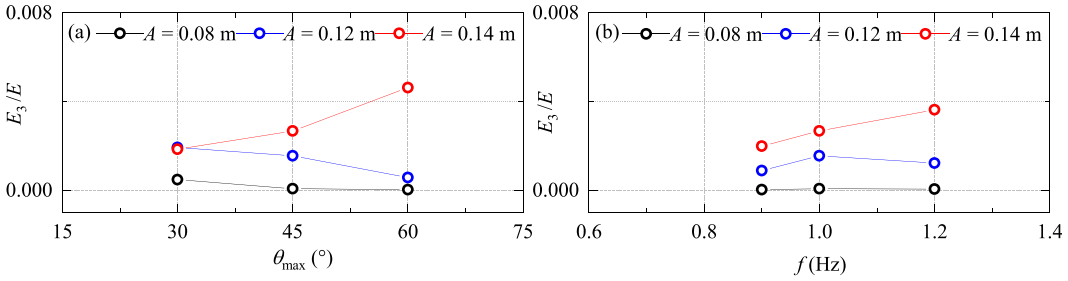

FIG. 13. Variation of the energy ratio of third-order terms. (a) With various directional distributions (with fixed frequency $f = 1.0$ Hz) and (b) with various frequencies (with fixed directional distribution $\theta_{max} = 45°$).

conclusion at $\theta_{max} = 60°$. This suggests that waves in actual sea conditions cannot be simplified as two-dimensional waves. That is to say, when considering the directional distribution, specific situations need to be handled on a case-by-case basis. It cannot be simply assumed that multi-directional waves are necessarily nonlinearly weakened compared to unidirectional waves.

For multi-directional waves, the impact of the directional distribution on geometric asymmetry does not follow the variation patterns observed in unidirectional waves. For larger focused amplitude (e.g., $A = 0.14$ m), as the directional distribution broadens, the period from the zero-upcrossing to the crest t_{cp}, the preceding horizontal asymmetry parameter β_p, and the trough-to-crest ratio exhibit a declining trend, while the vertical asymmetry factor λ show a significant increase. This indicates that the wider directional distribution in such configurations causes the wave profile to concentrate more energy on the preceding side of the wave crest, leading to a forward-leaning state with a rapidly growing crest and a much shallower trough, which signifies strong nonlinearity. Further analysis of harmonic energy supports this observation. In addition to the established relation between the trough-to-crest ratio and higher-order harmonics in unidirectional waves, t_{cp} appears to show greater more dependence on higher-order harmonics under the influence of directional distribution. Moreover, extending beyond previous research that suggested horizontal asymmetry is closely related to bound harmonics, β_p is shown to be more sensitive to the higher-order harmonics compared to β_f. Therefore, β_p can be identified as an indicator for evaluating the strength of higher-order nonlinearity.

In a summary, our research verifies the significant impact of directional distribution on the nonlinear characteristics of waves, as also noted by Johannessen and Swan.[62] Building on their work, we further investigated the dominant factors contributing to significant deformations in the preceding and following crest in multi-directional waves, identifying that the role of t_{cp} is more pronounced compared to t_{cf}. In addition, at the position of the largest wave crest (i.e., the actual focused position), the crest height on either side of the maximum are asymmetric, with the largest crest shifting toward the front of the wave group. This phenomenon is reflected in the variation of β_p (corresponding to the preceding wave-group envelop) in our study, confirming that the rate of dispersion is more rapid after the global maximum than it was before. Although we did not conduct an extremely detailed analysis in the spectral domain, we explained the impact of higher-order harmonics on larger waves influenced by directional distribution in a configuration with a uni-frequency wave component transitioning from multi-directional to be focused.

V. CONCLUSIONS

The multi-directional waves with uni-frequency which is missing in practical engineering are experimentally focused in the multifunctional wave basin. The influence of the directional distribution is analyzed and compared to that of the wave frequency. The main conclusions are summarized as follows:

(1) Different from the effect of the wave frequency, vertical asymmetry factor λ influenced by the directional distribution is associated with the variation of the period from the zero-upcrossing to the crest t_{cp}. Moreover, irrespective of the influence of the directional distribution or the wave frequency, $\theta_{max} = 45°$ is a special inflection point, for the different variations of λ on both sides.

(2) For wider directional distribution, there may still be a situation where the ratio of the following envelope height at half characteristic period β_f to the preceding β_p is greater than 1, known as a configuration highly prone to extreme events. More surprisingly, for relatively longer waves (i.e., $f = 0.9$ Hz) at $\theta_{max} = 45°$, the steeper the waves, the smaller the ratio β_f/β_p, which is contrary to the behavior observed in unidirectional waves. All these suggest that the nonlinearity of multi-directional waves is not necessarily weaker than that of unidirectional waves.

(3) Wave steepness defined in unidirectional waves is not available to measure the nonlinearity in multi-directional waves. It manifests as that in the configuration with $\theta_{max} = 45°$, the trough-to-crest ratio does increase with the increase of wave steepness in the corresponding unidirectional waves but exhibits non-monotonic characteristics.

(4) For multi-directional waves, particularly when the directional distribution θ_{max} exceeds 45°, the impact of the directional distribution and wave frequency on geometric asymmetry do not follow the variation patterns observed in unidirectional waves. When the focused amplitude reaches 0.14 m, the second- and third-order energy ratios at $\theta_{max} = 60°$ surpass those at $\theta_{max} = 45°$ and at $\theta_{max} = 30°$. The increase in harmonic energy leads to nonlinear enhancement, resulting in a decrease in the trough–crest asymmetry, manifested as a smaller value of trough-to-crest ratio. Contrary to conventional understanding, an increase in directional distribution is likely to lead to a decrease in wave nonlinearity.

The findings presented are based on the isolated impact of directional distribution and wave frequency, providing a reference for future research on the focusing of multi-directional multi-frequency wave components. This study also lays the groundwork for subsequent investigations, particularly concerning the asymmetric transformation between the temporal and spatial domains. Since wave nonlinearity encompasses not only the initial wave steepness but also the nonlinear interactions during wave propagation and evolution, it is preferable to examine information across more continuous locations rather than relying on simple or even nonlinear conversions between these two domains in the coming work.

ACKNOWLEDGMENTS

This work was supported by the National Natural Science Foundation of China (Nos. 52301319 and 52401324), the Guangdong Basic and Applied Basic Research Foundation (No. 2024A1515012321), the Guangzhou Basic and Applied Basic Research Foundation (No. 2023A04J1596), the Open Fund of State Key Laboratory of Coastal and Offshore Engineering, Dalian University of Technology (Nos. LP2304 and LP2403), the Ocean Youth Talent Project of Zhanjiang Science and Technology Bureau (No. 2021E05010), and the Doctoral Initiating Project of Guangdong Ocean University (No. 120602-R20069).

AUTHOR DECLARATIONS

Conflict of Interest

The authors have no conflicts to disclose.

Author Contributions

Yanli He: Conceptualization (equal); Data curation (equal); Funding acquisition (equal); Investigation (equal); Methodology (equal); Visualization (equal); Writing – original draft (equal). **Zhe Gao:** Data curation (equal); Investigation (equal); Visualization (equal). **Lei Wang:** Conceptualization (lead); Formal analysis (equal); Funding acquisition (equal); Methodology (lead); Writing – review & editing (lead). **Jinxuan Li:** Conceptualization (equal); Writing – review & editing (equal). **Guohai Dong:** Methodology (equal); Writing – review & editing (equal).

DATA AVAILABILITY

The data that support the findings of this study are available from the corresponding author upon reasonable request.

APPENDIX: EXPERIMENTAL REPEATABILITY VERIFICATION

To ensure the reproducibility of the experimental results and bolster confidence in the study's conclusions, it is essential to conduct repeatability and error verification. Figure 14 illustrates the comparison of water surface elevation at the defined focused position (also the actual focused position) using Case 1_1 from Table I as an example. The strong agreement between the time series from the first and second trials demonstrates the high repeatability of the laboratory experiments. Additionally, the relative error between the two experiments is statistics as 4.1%, which falls within the acceptable range of experimental errors, thereby ensuring the accuracy and reliability of the experimental data.

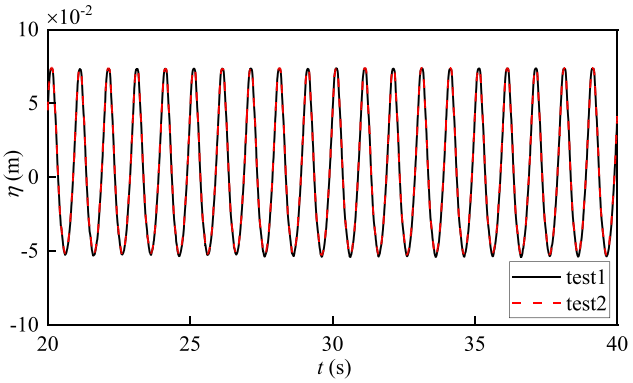

FIG. 14. Comparison of the water surface elevation at the defined focused position (also the actual focused position) tested Case 1_1 listed in Table I ($\theta_{max} = 30°$, $f = 1.0$ Hz, and $A = 0.14$ m) for repeatability verification.

REFERENCES

[1]M. L. McAllister, S. Draycott, R. Calvert, T. Davey, F. Dias, and T. S. van den Bremer, "Three-dimensional wave breaking," Nature **633**(8030), 601–607 (2024).
[2]L. Wang, K. L. X. Ding, B. Z. Zhou, P. Jin, S. X. Liu, J. H. Wang, and T. N. Tang, "Nonlinear statistical characteristics of the multi-directional waves with equivalent energy," Phys. Fluids **35**(8), 087101 (2023).
[3]T. N. Tang, W. T. Xu, D. Barratt, H. B. Bingham, Y. Li, P. H. Taylor, T. S. van den Bremer, and T. A. A. Adcock, "Spatial evolution of the kurtosis of steep unidirectional random waves," J. Fluid Mech. **908**, A3 (2021).
[4]B. Z. Zhou, K. L. X. Ding, J. S. Huang, L. Wang, J. L. Guo, and T. N. Tang, "Influence of uniform currents on nonlinear characteristics of double-wave-group focusing," Phys. Fluids **36**, 037125 (2024).
[5]M. Paprota and W. Sulisz, "Experimental study of freak wave formation in irregular wave trains propagating in water of constant depth," in 12th International Conference on Hydrodynamics, 2016.
[6]J. Zhang and M. Benoit, "Wave–bottom interaction and extreme wave statistics due to shoaling and de-shoaling of irregular long-crested wave trains over steep seabed changes," J. Fluid Mech. **912**, A28 (2021).
[7]M. Christou and K. Ewans, "Field measurements of rogue water waves," J. Phys. Oceanogr. **44**(9), 2317–2335 (2014).
[8]L. Wang, B. Z. Zhou, P. Jin, J. X. Li, S. X. Liu, and G. Ducrozet, "Relation between occurrence probability of freak waves and kurtosis/skewness in unidirectional wave trains under single-peak spectra," Ocean Eng. **248**, 110813 (2022).
[9]L. Wang, J. X. Li, S. X. Liu, and Y. P. Fan, "Experimental and numerical studies on the focused waves generated by double wave groups," Front. Energy Res. **8**, 133 (2020).
[10]C. Fochesato, S. Grilli, and F. Dias, "Numerical modeling of extreme rogue waves generated by directional energy focusing," Wave Motion **44**(5), 395–416 (2007).
[11]J. Zhang, M. Benoit, and Y. X. Ma, "Equilibration process of out-of-equilibrium sea-states induced by strong depth variation Evolution of coastal wave spectrum and representative parameters," Coastal Eng. **174**, 104099 (2022).
[12]D. A. G. Walker, P. H. Taylor, and R. E. Taylor, "The shape of large surface waves on the open sea and the Draupner New Year wave," Appl. Ocean Res. **26**(3–4), 73–83 (2004).
[13]V. Sriram, T. Schlurmann, and S. Schimmels, "Focused wave evolution using linear and second order wavemaker theory," Appl. Ocean Res. **53**, 279–296 (2015).

[14]C. Kharif and E. Pelinovsky, "Physical mechanisms of the rogue wave phenomenon," Eur. J. Mech. B **22**(6), 603–634 (2003).
[15]Y. L. He, Y. X. Ma, H. F. Mao, G. H. Dong, and X. Z. Ma, "Predicting the breaking onset of wave groups in finite water depths based on the Hilbert-Huang transform method," Ocean Eng. **247**, 110733 (2022).
[16]R. L. Fu, Y. X. Ma, G. H. Dong, and M. Perlin, "A new predictor of extreme events in irregular waves considering interactions of adjacent wave groups," Ocean Eng. **244**, 110441 (2022).
[17]A. F. Tao, J. H. Zheng, S. Mee Mee, and B. T. Chen, "The most unstable conditions of modulation instability," J. Appl. Math. **2012**, 1–11.
[18]G. H. Dong, R. L. Fu, Y. X. Ma, and K. Z. Fang, "Simulation of unidirectional propagating wave trains in deep water using a fully non-hydrostatic model," Ocean Eng. **180**, 254–266 (2019).
[19]R. J. Rapp and W. K. Melville, "Laboratory measurements of deep-water breaking waves," Philos. Trans. R. Soc. London, Ser. A **331**(1622), 735–800 (1990).
[20]K. Trulsen, A. Raustøl, S. Jorde, and L. Rye, "Extreme wave statistics of long-crested irregular waves over a shoal," J. Fluid Mech. **882**, R2 (2020).
[21]Y. L. He, G. L. Wu, H. F. Mao, H. Z. Chen, J. B. Lin, and G. H. Dong, "An experimental study on nonlinear wave dynamics for freak waves over an uneven bottom," Front. Mar. Sci. **10**, 1150896 (2023).
[22]Y. X. Ma, X. Z. Ma, M. Perlin, and G. H. Dong, "Extreme waves generated by modulational instability on adverse currents," Phys. Fluids **25**(11), 114109 (2013).
[23]D. Z. Ning, J. Du, X. L. Zhuo, J. Z. Liu, and B. Teng, "Harmonic energy transfer for extreme waves in current," China Ocean Eng. **31**(2), 160–166 (2017).
[24]M. A. Donelan and A. K. Magnusson, "The role of meteorological focusing in generating rogue wave conditions," in *Proceedings of the 14th Winter Workshop 'Aha Huliko,' Honolulu, USA* (University of Hawai'i at Mānoa, 2005), pp. 139–145.
[25]A. Regev, Y. Agnon, M. Stiassnie, and O. Gramstad, "Sea-swell interaction as a mechanism for the generation of freak waves," Phys. Fluids **20**, 112102 (2008).
[26]T. E. Baldock, C. Swan, and P. H. Taylor, "A laboratory study of nonlinear surface waves on water," Philos. Trans. R. Soc. London, Ser. A **354**(1707), 649–676 (1996).
[27]Y. X. Ma, G. H. Dong, S. X. Liu, J. Zang, J. X. Li, and Y. Y. Sun, "Laboratory study of unidirectional focusing waves in intermediate depth water," J. Eng. Mech. **136**(1), 78–90 (2010).
[28]S. X. Liang, Y. H. Zhang, Z. C. Sun, and Y. L. Chang, "Laboratory study on the evolution of waves parameters due to wave breaking in deep water," Wave Motion **68**, 31–42 (2017).
[29]D. Stagonas, E. Buldakov, and R. Simons, "Experimental generation of focusing wave groups on following and adverse-sheared currents in a wave-current flume," J. Hydraul. Eng. **144**(5), 04018016 (2018).
[30]R. Cao, E. M. Padilla, and A. H. Callaghan, "The influence of bandwidth on the energetics of intermediate to deep water laboratory breaking waves," J. Fluid Mech. **971**, A11 (2023).
[31]C. Guedes Soares, Z. Cherneva, and E. M. Antão, "Steepness and asymmetry of the largest waves in storm sea states," Ocean Eng. **31**(8–9), 1147–1167 (2004).
[32]R. S. Gibson and C. Swan, "The evolution of large ocean waves: The role of local and rapid spectral changes," Proc. R. Soc., Ser. A **463**(2077), 21–48 (2007).
[33]T. Vyzikas, D. Stagonas, E. Buldakov, and D. Greaves, "The evolution of free and bound waves during dispersive focusing in a numerical and physical flume," Coastal Eng. **132**, 95–109 (2018).
[34]J. L. Gao, L. H. Hou, Y. Y. Liu, and H. B. Shi, "Influences of Bragg reflection on harbor resonance triggered by irregular wave groups," Ocean Eng. **305**, 117941 (2024).
[35]T. N. Tang, P. S. Tromans, and T. A. A. Adcock, "Field measurement of nonlinear changes to large gravity wave groups," J. Fluid Mech. **873**, 1158–1178 (2019).
[36]J. L. Gao, C. L. Mi, Z. W. Song, and Y. Y. Liu, "Transient gap resonance between two closely-spaced boxes triggered by nonlinear focused wave groups," Ocean Eng. **305**, 117938 (2024).
[37]D. Myrhaug and S. P. Kjeldsen, "Parametric modelling of joint probability density distributions for steepness and asymmetry in deep water waves," Appl. Ocean Res. **6**(4), 207–220 (1984).
[38]H. F. Chen and Q. P. Zou, "Geometry of deep and intermediate water breaking waves influenced by wind speed and direction," Phys. Fluids **34**(8), 087126 (2022).
[39]D. Myrhaug and S. P. Kjeldsen, "Steepness and asymmetry of extreme waves and the highest waves in deep water," Ocean Eng. **13**(6), 549–568 (1986).
[40]L. Shemer and B. Dorfman, "Experimental and numerical study of spatial and temporal evolution of nonlinear wave groups," Nonlinear Processes Geophys. **15**, 931–942 (2008).
[41]M. S. Longuet-Higgins, "On the skewness of sea-surface slopes," J. Phys. Oceanogr. **12**, 1283–1291 (1982).
[42]A. Babanin, D. Chalikov, I. R. Young, and I. Savelyev, "Numerical and laboratory investigation of breaking of steep two-dimensional waves in deep water," J. Fluid Mech. **644**, 433–463 (2010).
[43]F. De Vita, R. Verzicco, and A. Iafrati, "Breaking of modulated wave groups: Kinematics and energy dissipation processes," J. Fluid Mech. **855**, 267–298 (2018).
[44]M. L. McAllister, N. Pizzo, S. Draycott, and T. S. van den Bremer, "The influence of spectral bandwidth and shape on deep-water wave breaking onset," J. Fluid Mech. **974**, A14 (2023).
[45]F. Fedele, M. L. Banner, and X. Barthelemy, "Crest speeds of unsteady surface water waves," J. Fluid Mech. **899**, A5 (2020).
[46]J. L. Gao, H. Z. Chen, L. L. Mei, Z. Liu, and Q. Liu, "Statistical analyses of wave height distribution for multidirectional irregular waves over a sloping bottom," China Ocean Eng. **35**(4), 504–517 (2021).
[47]T. A. A. Adcock, R. H. Gibbs, and P. H. Taylor, "The nonlinear evolution and approximate scaling of directionally spread wave groups on deep water," Proc. R. Soc., Ser. A **468**(2145), 2704–2721 (2012).
[48]R. Lakshman, V. Sriram, and V. Sundar, "Experimental investigation on the characteristics of directional focusing waves," Proc. Inst. Mech. Eng., Part M **237**(1), 20–36 (2023).
[49]T. B. Johannessen and C. Swan, "A laboratory study of the focusing of transient and directionally spread surface water waves," Proc. R. Soc. London, Ser. A **457**, 971–1006 (2001).
[50]M. Onorato, L. Cavaleri, S. Fouques, O. Gramstad, P. A. E. M. Janssen, J. Monbaliu, A. R. Osborne, C. Pakozdi, M. Serio, C. T. Stansberg, A. Toffoli, and K. Trulsen, "Statistical properties of mechanically generated surface gravity waves: A laboratory experiment in a three-dimensional wave basin," J. Fluid Mech. **627**, 235–257 (2009).
[51]A. Toffoli, O. Gramstad, K. Trulsen, J. Monbaliu, E. Bitner-Gregersen, and M. Onorato, "Evolution of weakly nonlinear random directional waves: Laboratory experiments and numerical simulations," J. Fluid Mech. **664**, 313–336 (2010).
[52]W. T. Xiao, Y. M. Liu, G. Y. Wu, and D. K. P. Yue, "Rogue wave occurrence and dynamics by direct simulations of nonlinear wave-field evolution," J. Fluid Mech. **720**, 357–392 (2013).
[53]D. Barratt, H. B. Bingham, P. H. Taylor, T. S. van den Bremer, and T. A. A. Adcock, "Rapid spectral evolution of steep surface wave groups with directional spreading," J. Fluid Mech. **907**, A30 (2021).
[54]M. Onorato, D. Proment, and A. Toffoli, "Freak waves in crossing seas," Eur. Phys. J. Spec. Top. **185**(1), 45–55 (2010).
[55]A. Toffoli, E. M. Bitner-Gregersen, A. R. Osborne, M. Serio, J. Monbaliu, and M. Onorato, "Extreme waves in random crossing seas: Laboratory experiments and numerical simulations," Geophys. Res. Lett. **38**(6), L06605, https://doi.org/10.1029/2011GL046827 (2011).
[56]A. D. Sabatino and M. Serio, "Experimental investigation on statistical properties of wave heights and crests in crossing sea conditions," Ocean Dyn. **65**(5), 707–720 (2015).
[57]P. G. Petrova and C. Guedes Soares, "Distributions of nonlinear wave amplitudes and heights from laboratory generated following and crossing bimodal seas," Nat. Hazards Earth Syst. Sci. **14**(5), 1207–1222 (2014).
[58]M. L. McAllister, S. Draycott, T. A. A. Adcock, P. H. Taylor, and T. S. van den Bremer, "Laboratory recreation of the Draupner wave and the role of breaking in crossing seas," J. Fluid Mech. **860**, 767–786 (2019).
[59]S. Haver, "Evidences of the existence of freak waves," in Rogues Waves 2000, Brest, France, 2000.
[60]X. R. Ji, S. X. Liu, J. X. Li, and W. Jia, "Experimental investigation of the interaction of multidirectional irregular waves with a large cylinder," Ocean Eng. **93**, 64–73 (2015).
[61]H. C. Zhang, S. X. Liu, J. X. Li, and J. Hao, "Interactions between multidirectional irregular waves and a pile group in a side-by-side arrangement: Probabilistic analysis," Coastal Eng. **165**, 103851 (2021).

[62]T. B. Johannessen and C. Swan, "on the nonlinear dynamics of wave groups produced by the focusing of surface-water waves," Proc. R. Soc. London, Ser. A **459**(2032), 1021–1052 (2003).
[63]C. H. Wu and H. M. Nepf, "Breaking criteria and energy losses for three-dimensional wave breaking," J. Geophys. Res. **107**(C10), 3177, https://doi.org/10.1029/2001JC001077 (2002).
[64]T. A. A. Adcock, P. H. Taylor, and S. Draper, "Nonlinear dynamics of wave-groups in random seas: Unexpected walls of water in the open ocean," Proc. R. Soc., Ser. A **471**(2184), 20150660 (2015).
[65]M. L. Banner, X. Barthelemy, F. Fedele, M. Allis, A. Benetazzo, F. Dias, and W. L. Peirson, "Linking reduced breaking crest speeds to unsteady nonlinear water wave group behavior," Phys. Rev. Lett. **112**(11), 114502 (2014).
[66]M. A. Tayfun, "On narrow-band representation of ocean waves 1. Theory," J. Geophys. Res. Oceans **91**(C6), 7743–7752, https://doi.org/10.1029/JC091iC06p07743 (1986).
[67]G. H. Dong, X. Gao, X. Z. Ma, and Y. X. Ma, "Energy properties of regular water waves over horizontal bottom with increasing nonlinearity," Ocean Eng. **218**, 108159 (2020).
[68]K. She, C. A. Greated, and W. J. Easson, "Experimental study of three-dimensional wave breaking," J. Waterw., Port, Coastal Ocean Eng. **120**(1), 20–36 (1994).
[69]M. Perlin, W. Y. Choi, and Z. G. Tian, "Breaking waves in deep and intermediate waters," Annu. Rev. Fluid Mech. **45**(1), 115–145 (2013).
[70]A. F. Yao and C. H. Wu, "Spatial and temporal characteristics of transient extreme wave profile on depth-varying currents," J. Eng. Mech. **132**(9), 1015–1025 (2006).
[71]Z. G. Tian, M. Perlin, and W. Y. Choi, "Frequency spectra evolution of two-dimensional focusing wave groups in finite depth water," J. Fluid Mech. **688**(1), 169–194 (2011).